Available online at www.sciencedirect.com

SciVerse ScienceDirect

Ceramics International 39 (2013) 4953–4960

CERAMICS INTERNATIONAL

www.elsevier.com/locate/ceramint

Dolomite, wollastonite and calcite as different CaO sources in anorthite-based porcelain

Shanjun Ke, Xiaosu Cheng*, Yanmin Wang, Qianghong Wang, Hui Wang

College of Materials Science and Engineering, South China University of Technology, Guangzhou 510640, China

Received 23 October 2012; received in revised form 26 November 2012; accepted 27 November 2012
Available online 5 December 2012

Abstract

Anorthite-based porcelain was fabricated by using ball clay, quartz, alumina, feldspar and three different sources of CaO as raw materials. The effect of CaO sources such as dolomite, wollastonite and calcite on the mechanical, thermal and aesthetical properties of anorthite-based porcelain was investigated. X-ray diffraction (XRD) and scanning electron microscopy (SEM) studies were also carried out to analyze the microstructure. Anorthite was formed as major phase in all the samples fired at their optimum sintering temperatures (1200, 1215 and 1230 °C). The sample with dolomite had the highest bulk density but the smallest flexural strength due to formation of substantial glassy phase. The maximum flexural strength (~110 MPa) was reached in the sample containing wollastonite, which was mainly attributed to the favorable microstructure. Anorthite as the single crystalline phase was found in the sample with calcite and the sample showed the lowest thermal expansion coefficient and the highest whiteness, which was similar to bone china in appearance.

Keywords: D. Porcelain; Anorthite; CaO sources

1. Introduction

Bone china is a highly specialized product in terms of its appearance; being exceptionally white and translucent makes it the world's most expensive type of tableware [1]. Typical composition of bone china is about 50 wt% animal bone ash, 25 wt% china clay and 25 wt% Cornish stone or feldspar [2]. After sintering, the phases in the fired body generally consist of 40 wt% β-tricalcium phosphate (β-$Ca_3(PO_4)_2$), 30 wt% anorthite ($CaO \cdot Al_2O_3 \cdot 2SiO_2$), and 30 wt% calcium aluminosilicate glass phase [3,4]. So, bone china is a highly crystalline (~70%) whiteware that exhibits good resistance to edge chipping and a high flexural strength value of ~100 MPa [5,6].

However, the glaze applied to bone china is easily scratched and the fired body thermal shock resistance is poor. The former is due to its alkaline rich glaze and the latter is attributed to mismatch of thermal expansion coefficient (TEC) of different phases in the fired body. The TEC of anorthite [7] from 20 to 500 °C is $\sim 4.3 \times 10^{-6}$ K^{-1}. The TEC of glass phase detected in bone china from 20 to 350 °C is calculated to be 3–4.5×10^{-6} K^{-1}, while the approximate TEC of β-tricalcium phosphate from 50 to 400 °C is 12×10^{-6} K^{-1} [8]. Apparently, β-tricalcium phosphate crystalline phase has a negative effect on thermostability of bone china. Meanwhile, anorthite has a refractive index of ~1.58 [9], which is close to that of the glass phase (~1.5) [10]. That is, anorthite crystalline phase can increase translucency performance of bone china. Therefore, anorthite-based porcelain can be used in tableware to improve heat stability and decoration quality.

In recent years, many studies [10–15] have been undertaken to develop anorthite-based porcelain to replace traditional porcelain (including bone china and hard porcelain). Capoglu [10–12] designed low-clay translucent whiteware, which was produced from prefired materials and a small amount of clay at 1370 °C for 3 h. The low-clay whiteware consisted of anorthite, mullite ($3Al_2O_3 \cdot 2SiO_2$) crystalline phases and glassy phase with high crystalline to glassy phase ratio. Taskiran [13,14] also reported a new porcelaneous stoneware, which was obtained from a mixture of wollastonite, alumina, quartz, magnesia and ball clay by powder pressing and sintering at 1225 °C. The material had anorthite

*Corresponding author. Tel.: +86 20 87114217; fax: +86 20 87110273.
E-mail address: guangzhouscut@163.com (X. Cheng).

0272-8842/$ - see front matter © 2012 Elsevier Ltd and Techna Group S.r.l. All rights reserved.
http://dx.doi.org/10.1016/j.ceramint.2012.11.091

as its major phase with corundum, cristobalite and glass as minor phase.

In addition, aluminous cement ($CaO \cdot Al_2O_3$ and $CaO \cdot 2Al_2O_3$), limestone ($CaCO_3$), colemanite ($2CaO \cdot 3B_2O_3 \cdot 5H_2O$), wollastonite ($CaO \cdot SiO_2$), calcite ($CaCO_3$) and dolomite ($CaCO_3 \cdot MgCO_3$) can all be used in the production of anorthite-based porcelains as a CaO source [16–20]. Meanwhile, the production of anorthite ceramics was studied with different sources of CaO such as $Ca(OH)_2$, $CaCO_3$, marble powder and gypsum mold waste by Kurama [21]. However, the above mentioned study only aimed to produce dense anorthite ceramics from different CaO sources, and there was little attention paid to the microstructure and the other properties. For tableware, the applicability and decoration quality is very important for its marketing. So, not all calcium-containing minerals are appropriate for the manufacture of anorthite-based porcelain for daily use. In China, dolomite, wollastonite and calcite are rather abundant, and are cheaper than other calcium-containing minerals. In a previous study [22], the preparation of anorthite-based porcelain was fabricated using calcite as a source of CaO. The present work, which is a part of an extended research program, aims to elucidate the influence of dolomite, wollastonite and calcite on the microstructure and technological properties of anorthite-based porcelain, including sintering character, flexural strength, thermal expansion and appearance quality.

2. Experimental procedure

2.1. Raw materials

Ball clay and quartz were used as starting raw materials. Dolomite, wollastonite and calcite were chosen as different CaO sources. Feldspar was used to obtain dense porcelain body at a relatively low temperature. The high content of CaO decreases the liquid phase viscosity of the porcelain at high temperatures, which makes it particularly easy to generate shape distortion of the porcelain bodies. To resist high-temperature deformation, a small amount of industrial alumina is added as a source of aluminum to increase the viscosity of high-temperature melted liquid. The starting raw materials were purchased from Guangdong Sitong Group Co. Ltd. (Chaozhou, China). Table 1 shows the chemical composition of raw materials.

2.2. Sample preparation

Compositions were prepared on the basis of the approximate stoichiometric anorthite compositions with different CaO sources (dolomite, wollastonite and calcite) and were labeled as A, B and C (Table 2), respectively. These powders were wet mixed and milled in a planetary mixer with zirconia ball millstone for 6 h. The particle size distributions of the milled slurry were analyzed by a BT-9300S model laser diffraction particle size analyzer (Dangdong Bettersize Instruments Ltd., China). The result is given in Fig. 1. It can be seen that all samples have approximate results with similar log-normal distribution presenting one maximum point. Meanwhile, the particle sizes are less than 10 μm, which are centered at 1–5 μm.

The slip casting was used for forming, which could obtain green body with high-strength [19]. Slips were cast in a plaster mold into rectangular blocks of 60 mm × 60 mm × 10 mm dimensions. The consolidated rectangular blocks were removed from the mold after 45 min. Natural drying time of the consolidated specimens was determined

Table 1
Chemical composition of raw materials.

Raw materials	Constituents (wt%)								
	SiO_2	Al_2O_3	Fe_2O_3	TiO_2	CaO	MgO	K_2O	Na_2O	L.O.I
Ball clay	48.61	36.14	0.21	0.14	0.16	0.21	0.98	0.24	12.7
Quartz	98.38	1.02	0.03	0.01	0.08	0.02	0.07	0.04	0.23
Alumina	–	≥99.0	–	–	–	–	–	–	–
Feldspar	65.56	18.85	0.08	0.02	0.23	0.03	12.39	2.28	0.56
Dolomite	1.32	0.45	0.04	0.03	29.90	19.41	0.02	0.36	48.46
Wollastonite	50.13	0.92	0.20	0.02	44.80	0.82	–	–	3.21
Calcite	3.02	0.61	0.04	0.01	53.98	2.13	0.04	0.11	39.82

Table 2
Composition of the investigated samples A, B and C (wt%).

Sample	Raw materials						
	Ball clay	Quartz	Alumina	Feldspar	Dolomite	Wollastonite	Calcite
A	20	14	21	–	45	–	–
B	20	7	15	18	–	40	–
C	20	20	12	18	–	–	30

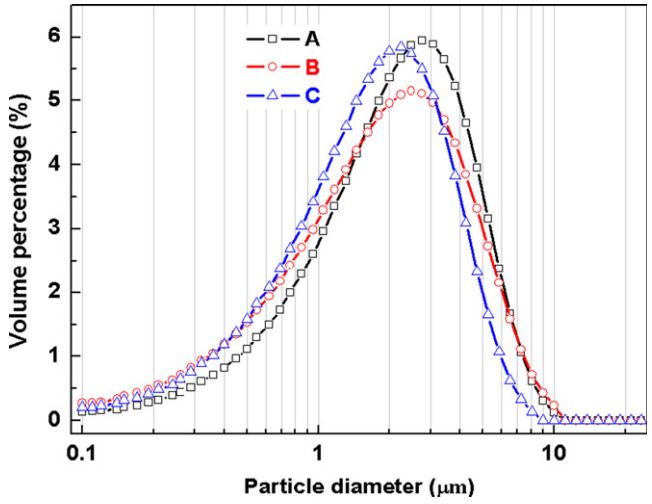

Fig. 1. Particle size distributions of samples A, B and C milled for 6 h.

for 24 h in air at room temperature and then the specimens were dried in an oven for 12 h at 90 °C. Subsequently, the specimens were processed into required size (5 mm × 5 mm × 55 mm) by cutting. The firing was performed in an electric furnace at a temperature from 1155 to 1260 °C for 1 h.

2.3. Measurements and analyses

The bulk density and water absorption of the fired body were determined by the Archimedes method according to ASTM C373 [23]. The flexural strength of samples (3 mm × 4 mm × 50 mm) as measured using an electronic universal tester (Model 5569, Instron Ltd.) by a three point bending fixture span of 30 mm and cross head speed of 0.5 mm/min. The thermal analysis was investigated by differential scanning calorimetry (DSC, STA449C, Netzsch Instruments Ltd., Germany), at a heating rate of 10 K/min, under air atmosphere. The thermal expansion coefficient of sintered specimens was determined between room temperature and 500 °C using an automatic dilatometer (DIL402EP, Netzsch Instruments Ltd., Germany), at a heating rate of 10 K/min. The crystalline phases were determined by an X-ray diffractometer (XRD, Philips PW-1710, the Netherlands), using Cu$K\alpha$ radiation. The microstructures were observed by a scanning electron microscope (SEM, Philips L30FEG, the Netherlands). The $L^*a^*b^*$ color parameters of samples were measured using a differential colorimeter (X-Rite Color Premier 8200, USA).

3. Results and discussion

The XRD patterns of samples fired at the optimal firing temperature are shown in Fig. 2. Obviously, anorthite is the primary crystalline phase, presenting some glassy phases in all samples. Akermanite ($2CaO \cdot MgO \cdot 2SiO_2$) and spinel ($MgO \cdot Al_2O_3$) are observed only in sample A, because dolomite is not only a kind of CaO source, but also a source of MgO. The akermanite-based glass–ceramic was

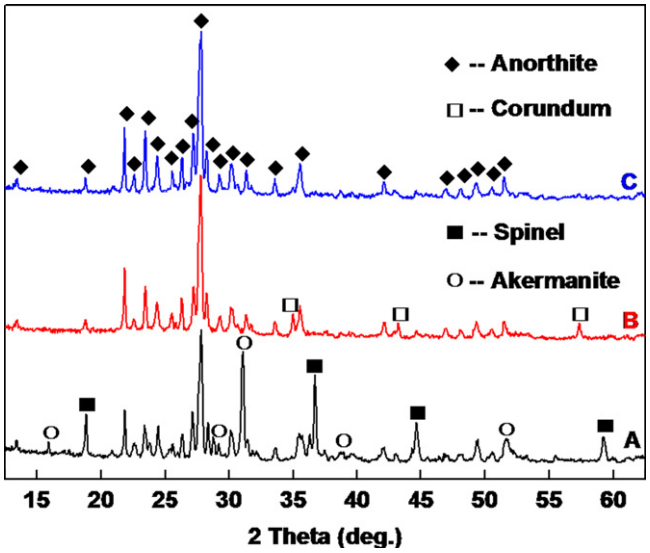

Fig. 2. XRD patterns of samples A, B and C fired at 1200 °C, 1215 °C and 1230 °C respectively.

Table 3
XRF chemical analysis result of the fired samples A, B and C.

Sample	Oxides (wt%)							
	SiO_2	Al_2O_3	Fe_2O_3	TiO_2	CaO	MgO	K_2O	Na_2O
A	32.10	37.47	0.11	0.03	18.00	11.70	0.29	0.28
B	48.66	29.83	0.16	0.03	18.83	0.39	1.77	0.33
C	49.60	26.79	0.09	0.03	19.20	0.81	2.89	0.58

prepared from the SiO_2–Al_2O_3–B_2O_3–MgO–CaO–Na_2O–F system by Ventura [24]. Literature [25] also reported that the phases of anorthite, spinel and mullite ($3Al_2O_3 \cdot 2SiO_2$) were generated from kaolin–dolomia mixtures. Moreover, anorthite as the single crystalline phase is obtained in the sample C while a small amount of corundum (Al_2O_3) crystalline phase is shown in Fig. 2B, which can be explained with a content of Al_2O_3 in sample B higher than that of the sample C in Table 3.

Differential scanning calorimetry (DSC) is used to study all the transformations involving heat exchange occurring in a material during a heating cycle. Therefore, it is a suitable technique for identifying phenomena such as phase transitions, crystallization or melting. Fig. 3 shows the DSC curves of samples A, B and C at temperatures from ambient temperature to 1250 °C. Clearly, the tendency of all DSC curves is consistent, when the temperature is below 600 °C. There is one exothermic peak at around 350 °C and two endothermic peaks at around 500 and 576 °C. The exothermic peak is related to the combustion of the organic matter, which is a component of the ball clay, and the first endothermic peak corresponds to the matrix dehydroxylation process according to the following reaction [26]:

$$Al_2O_3 \cdot 2SiO_2 \cdot 2H_2O(\text{kaolinite}) \rightarrow Al_2O_3 \cdot 2SiO_2(\text{metakaolinite}) + 2H_2O \quad (1)$$

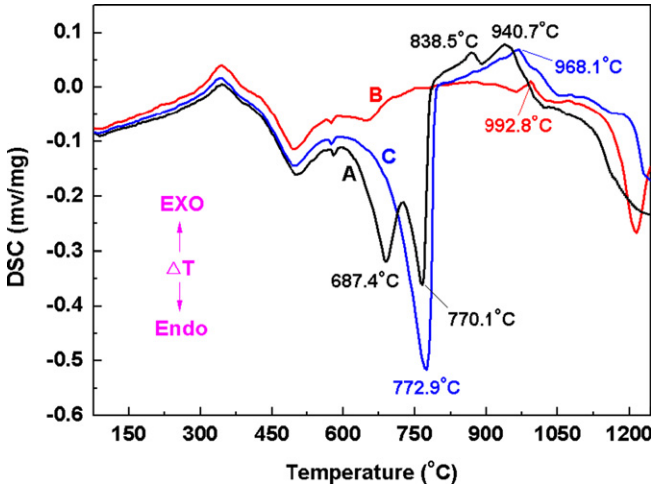

Fig. 3. DSC curves of samples A, B and C.

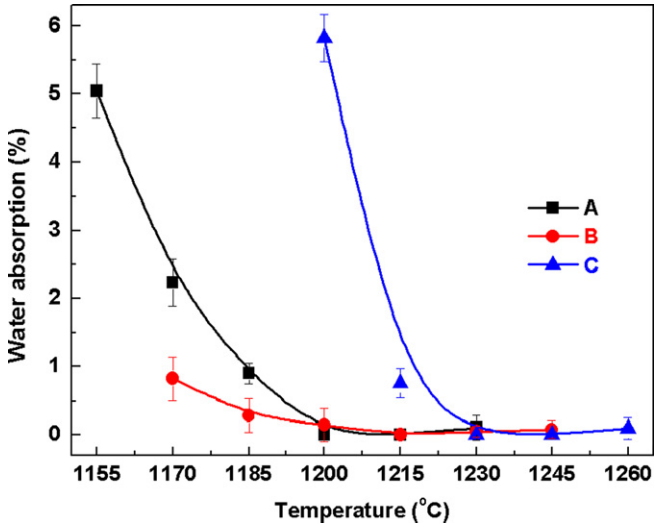

Fig. 4. Water absorption variation of samples A, B and C as a function of temperature.

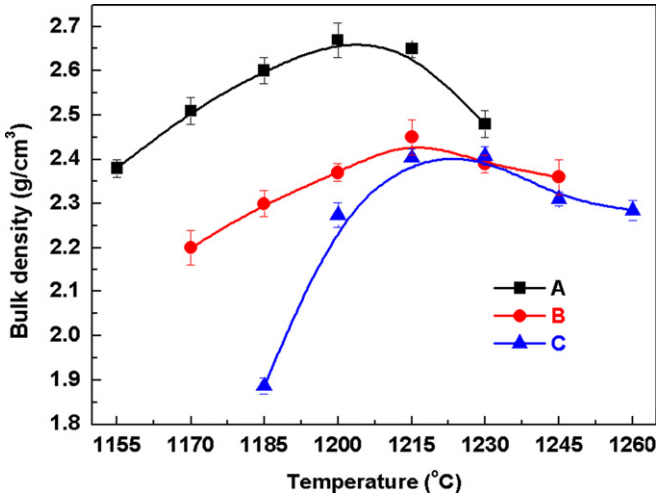

Fig. 5. Bulk density variation of samples A, B and C as a function of temperature.

For the third peak, the small endothermic peak was attributed to α- to β-quartz transition.

Above 600 °C, the DSC curves of samples A, B and C have great differences. On the curve A, two endothermic peaks and two exothermic peaks are observed at 687, 770, 838 and 940 °C. Two sharp endothermic peaks were assigned to dolomite and calcite decarbonation. In another work [27], the reaction process was researched by Lagzdina in detail; related reactions are as follows:

$$CaMg(CO_3)_2(\text{dolomite}) \rightarrow CaCO_3(\text{calcite}) + MgO + CO_2 \quad (2)$$

$$CaCO_3(\text{calcite}) \rightarrow CaO + CO_2 \quad (3)$$

And the exothermic peaks occurred from crystallization of new crystals, including anorthite, akermanite and spinel (Fig. 2). According to the thermal analysis results, samples B and C showed some differences compared with sample A. On the curve B, the exothermic peak was observed at 992 °C due to an unknown crystal formation. On the curve C, one drastic endothermic peak and one exothermic peak were observed at 773 and 968 °C, respectively. The former corresponds to the decomposition of $CaCO_3$, while the latter indicates the formation of anorthite (Fig. 2). Furthermore, as seen from Fig. 3, they present steep slope indicating the formation of high-temperature melt suddenly between 1000 and 1200 °C. In general, the melted glassy phase plays a flux role and makes the material increase bulk density easily [19].

Fig. 4 shows the behavior of the water absorption as a function of temperature. The water absorption decreases with increase in heating temperature due to reduction of the apparent porosity through liquid phase sintering. Samples A, B and C reach a value of water absorption of 0.00% at the firing temperatures of 1200, 1215 and 1230 °C, respectively. Fig. 5 displays the variation in bulk density with heating temperature. At first, the bulk density value continues to increase, and optimum values are achieved when the water absorption reached a minimum value tending to be nearly zero. Further firing results in a small fall of bulk density mainly due to expansion of the entrapped gases, that is, blisters and bloating [28].

Moreover, it can be seen from Fig. 5 that sample A has significant difference compared with samples B and C. Sample A has the highest bulk density (2.67 g cm^{-3}). The maximum bulk density of sample B is 2.45 g cm^{-3}, and 2.41 g cm^{-3} for sample C. Table 4 summarizes the important physical properties of crystalline phases identified in this study. Sample A has the highest density value due to formation of a substantial spinel phase (3.58 g cm^{-3}) [29]. For the same reason, a small amount of corundum (4.05 g cm^{-3}) [28] makes the density of sample B higher than that of sample C.

Fig. 6 shows the flexural strength behavior as a function of sintering temperature. The flexural strength of all samples increases with an increase in sintering temperature. On further heating, the flexural strength values reach

maximum values of around 85 MPa for sample A, 100 MPa for sample B, and 110 MPa for sample C and then decrease with a corresponding decrease in density. Theoretically, flexural strength developed in a porcelain body is maximum when apparent porosity decreases to zero. A similar result is observed in the present study. Furthermore, according to Figs. 4 and 6, an abnormal phenomenon is found where sample A has the highest density but the smallest strength. The low strength of sample A can be explained by the substantial glassy liquid formation due to high content of MgO (11.7 wt%).

Porosity and microstructure are considered important parameters regarding the mechanical properties of fired porcelain body. Fig. 7 shows SEM micrographs of the polished surface of samples A, B and C fired at their optimal firing temperatures. Sample A presents larger, isolated, spherical pores in the range of 30–40 μm (Fig. 7A). Samples B and C are characterized by small isolated pores (10–20 μm), which are less spherical (elongated or ellipsoid). Additionally, sample C presents a larger number of pores than sample B, which is due to calcite decarbonation generating residual entrapped gas. Thus, a clear relation between strength and porosity can be confirmed. That is, high porosity and big flaw sizes are unfavorable to the strength of fired porcelain body.

The SEM images of the fracture surface of samples chemically etched with hydrofluoric acid for 30 s are shown in Fig. 8. Characteristic octahedral spinel crystals are clearly seen in Fig. 8A. Akermanite and anorthite are not easily recognizable due to their being surrounded by a large amount of glass phase. In Fig. 8B, very small anorthite crystals together with a small amount of glassy phase are observed. Lamellar crystals of anorthite are cemented with residual glass, and the grain sizes are less than 3 μm (Fig. 8C). Marques [30] also fabricated anorthite crystals with similar shape. Comparing Fig. 8A, B and C, it is easy to make a qualitative comparison for the content of the residual glass phase. And it follows the general order $C < B < A$. So, sample C possesses a high crystalline to glass ratio, which also may show high strength [31–33].

The thermal expansion coefficient (TEC) is a key factor when considering the thermal matching between glaze and body [34]. Fig. 9 shows the TEC curves of samples A, B and C measured over the temperature range from 30 to 500 °C using a dilatometer. The expansion ratios have almost linear increase over the entire measured temperature range. For practical application of high-strength porcelain for tableware, thermal expansion below 150 °C is important in order to withstand the thermal shock of heat disinfection or washing [35]. According to thermal expansion coefficients, the average TEC values of all the samples in the area of the tested temperature are calculated and listed in Table 5. From the table, the TEC of samples A, B and C below 300 °C were calculated as $7.2 \times 10^{-6}\,K^{-1}$, $5.1 \times 10^{-6}\,K^{-1}$ and $4.9 \times 10^{-6}\,K^{-1}$, respectively. According to the simple rule of mixtures [1], the value of TEC could be calculated by using simple rule of mixtures which is consistent with the relative proportions of the phases. Sample A has a high TEC because of the presence of akermanite ($10.3 \times 10^{-6}\,K^{-1}$) [36] and spinel ($8.2 \times 10^{-6}\,K^{-1}$) [34]. A small amount of corundum ($7–8 \times 10^{-6}\,K^{-1}$) [37] crystalline phase has a negative effect on decreasing the TEC of sample B. Sample C has a low TEC value of $4.9 \times 10^{-6}\,K^{-1}$ due to the formation of a single anorthite phase, whose TEC value is $\sim 4.3 \times 10^{-6}\,K^{-1}$ from 20 to 500 °C [7], while the TEC for glasses of the compositions detected in common glaze [1] from 20 to 350 °C were calculated to be $3–4.5 \times 10^{-6}\ K^{-1}$. Therefore, samples B

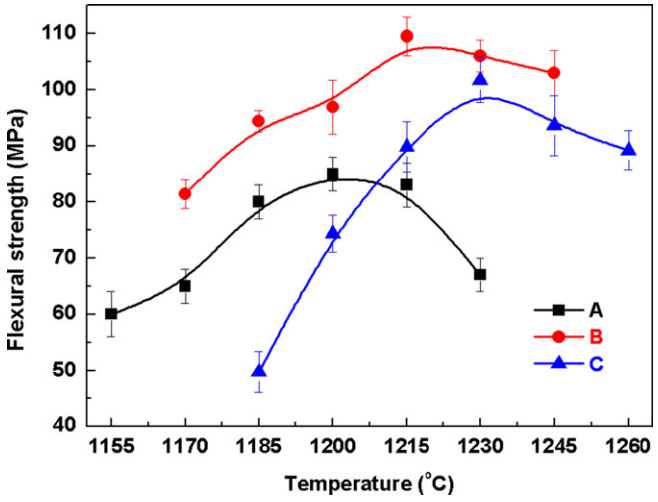

Fig. 6. Flexural strength variation of samples A, B and C as a function of temperature.

Table 4
Crystalline phases of samples A, B and C fired at 1200 °C, 1215 °C and 1230 °C respectively.

Sample	Temperature (°C)	Crystalline phases	Physical property		
			Density (g cm^{-3})	TEC × 10^{-6} (K^{-1})	Refractive index
A	1200	Anorthite	2.76	4.5	1.58
		Akermanite	2.95	10.3	1.64
		Spinel	3.58	8.2	1.72
B	1215	Anorthite	2.76	4.5	1.58
		Corundum	4.05	7–8	1.76
C	1230	Anorthite	2.76	4.5	1.58

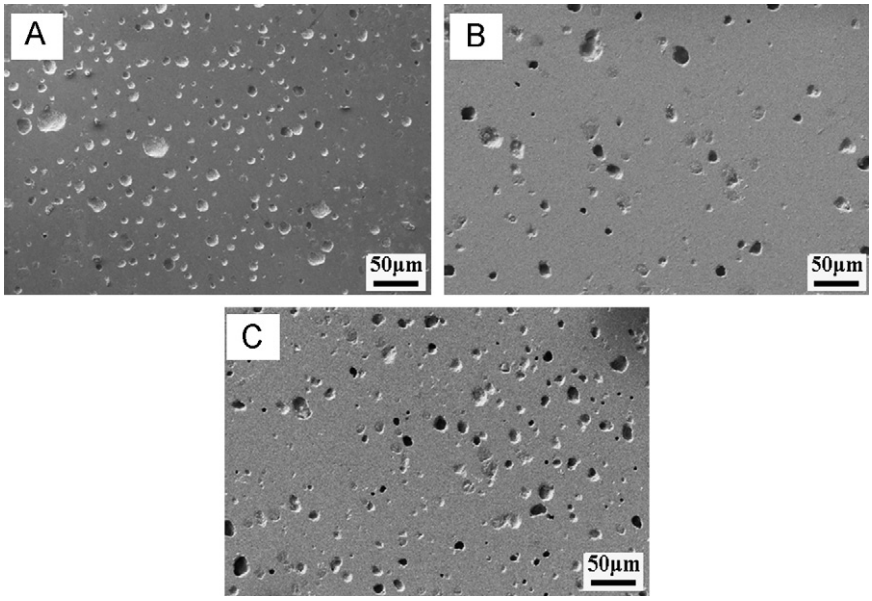

Fig. 7. Pore structures of samples A, B and C fired at 1200 °C, 1215 °C and 1230 °C respectively.

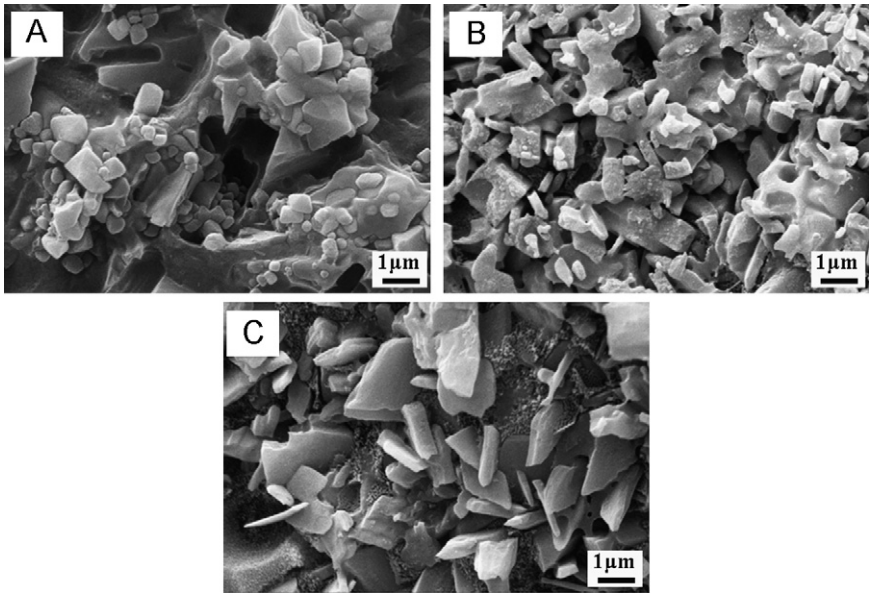

Fig. 8. SEM images of the fracture surface of samples A, B and C fired at 1200 °C, 1215 °C and 1230 °C respectively.

and C can be matched with applicable glaze easily. Moreover, this relatively low TEC also indicates that the materials would be very resistant to being thermally shocked.

In modern technology for the production of vitrified porcelainware, particularly for tableware, greater attention is paid to the whiteness of porcelain body [38]. In the present study, the color of fired body was measured using a spectrometer used in the reflection mode. The $L^*a^*b^*$ system was chosen for this study because it best quantifies color as perceived by the human eye [39]. As is known to all, bone china has the most excellent appearance such as translucency and whiteness [40]. In order to explain quantitatively the effect on the degree of whiteness, the values of three types of anorthite-based ceramic were compared with commercially produced bone china. The color difference values (a^*, b^*) and the L^* parameters (whiteness) are represented in Table 6. The a^* parameter reflects the scale extending from green ($-a^*$) to red ($+a^*$), while the b^* parameter reflects the scale extending from blue ($-b^*$) to yellow ($+b^*$). It can be seen that negative value of a^* and positive value of b^* were measured from all samples, indicating that the values lie in the upper left quadrant (green and yellow region) with coordinates. A lower value of a^* and b^* on sample C indicates that there is very low coloring grade. Meanwhile, the degree of whiteness of sample C can reach $\sim$94, which is the highest of all the samples due to the lowest content of coloring impurities such as Fe_2O_3 and

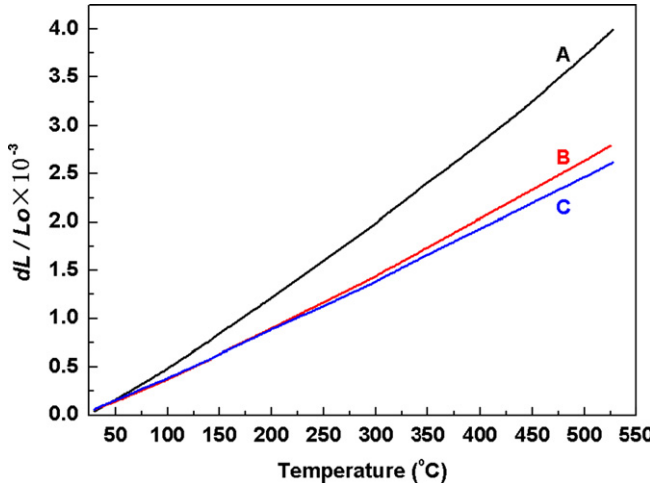

Fig. 9. Thermal expansion ratio curves of samples A, B and C measured in the range from 30 to 500 °C.

Table 5
Average TEC values of samples A, B and C measured in the range from 30 to 500 °C.

Temperature (°C)	Thermal expansion coefficient, $\alpha \times 10^{-6}(K^{-1})$		
	A	B	C
30–100	6.2748	4.4888	4.6472
30–200	6.9009	4.9382	4.8745
30–300	7.2094	5.1233	4.9142
30–400	7.4943	5.3458	5.0601
30–500	7.8267	5.4822	5.1189

Table 6
$L^*a^*b^*$ parameters of samples A, B, C and bone china.

Sample code	Color coordinate		
	L^*	a^*	b^*
A	92.59	−1.47	4.31
B	91.01	−0.89	4.86
C	94.37	−0.54	1.92
Bone china	93.15	−0.43	3.17

TiO_2 for raw materials. Moreover, a lower glassy phase formed in sample C may be another reason for high whiteness. The literature [13] has also explained that the glassy phase had a negative effect on the increase in whiteness of anorthite-based stoneware. Therefore, sample C has a higher appearance quality superior to bone china [5].

The translucency behavior of tableware is also crucial for its marketing. Theoretically, the translucency behavior of material is related to light scattering, which can cause a bad influence on transmittance. For the traditional ceramic, matching refractive indices between different phases can reduce scattering losses. This approach is used in making high-quality bone china [41]. Even though the translucency has not been measured quantitatively, the result can be got by theoretical analysis of relative refractive index difference with different phases. For sample C, there is only one crystalline phase and the anorthite crystal has a refractive index value of 1.58 [9], which is close to that of the glass phase. So, sample C shows excellent translucency behavior which could achieve a high-quality decorative effect similar to bone china. On the contrary, the relatively larger difference in refractive index [42] could cause a negative effect on the translucency behavior of samples A and B because of the presence of multiphase.

4. Conclusions

Anorthite-based porcelains were prepared by using three different CaO sources including dolomite, wollastonite and calcite. Effect of different CaO sources on the microstructure and technological properties such as sintering behavior, flexural strength, thermal expansion and appearance quality was investigated. The experimental results showed that the microstructure and property of porcelain were affected by different CaO sources.

Anorthite was the primary crystalline phase in all samples fired at optimum sintering temperatures (1200, 1215 and 1230 °C). Anorthite as the single crystalline phase was only generated from the sample including calcite and the single anorthite porcelain possessed high crystalline to glassy phase ratio. The sample containing dolomite easily formed substantial glassy phase due to the existence of magnesium element. The maximum flexural strength could reach ~110 MPa when the source of CaO was wollastonite, which was attributed to relatively advantageous microstructure.

When the source of CaO was wollastonite or calcite, the anorthite-based porcelain has low thermal expansion coefficient due to formation of substantial anorthite phase, which could be matched with applicable glaze easily. The single anorthite porcelain had high whiteness ($L^*=94$). Moreover, the relatively low refractive index value between anorthite and glassy phase would facilitate the attainment of high translucency behavior, which was similar to bone china in appearance.

Acknowledgments

This work was supported by the Major Scientific and Technological Projects of Guangdong Province (No. 2010A080804001) and the ChanXueYan Special Funds of Guangdong (No. 2011B090400201).

References

[1] A. Capoglu, Elimination of discoloration in reformulated bone china bodies, Journal of the European Ceramic Society 25 (2005) 3157–3162.
[2] S.A.F. Batista, P.F. Messer, R.J. Hand, Fracture toughness of bone china and hard porcelain, British Ceramic Transactions 10 (2001) 256–259.
[3] A. Kara, R. Stevens, Characterisation of biscuit fired bone china body microstructure. Part II: transmission electron microscopy (TEM) of glassy matrix, Journal of the European Ceramic Society 22 (2002) 737–743.

[4] C.B. Ustundag, Y.K. Tur, A. Capoglu, Mechanical behavior of a low-clay translucent whiteware, Journal of the European Ceramic Society 26 (2006) 169–177.
[5] A. Capoglu, A novel low-clay translucent whiteware based on anorthite, Journal of the European Ceramic Society 31 (2010) 321–329.
[6] X.S. Cheng, S.J. Ke, Q.H. Wang, H. Wang, A.Z. Shui, P.A. Liu, Characterization of transparent glaze for single-crystalline anorthite, Ceramics International 38 (2012) 4901–4908.
[7] B. Ryu, I. Yasui, Sintering and crystallization behavior of a glass powder and block with a composition of anorthite and the microstructure dependence of its thermal expansion, Journal of Materials Science 29 (1994) 3323–3328.
[8] Y. Iqbal, P.F. Messer, W.E. Lee, The non-equilibrium microstructure of bone china, British Ceramic Transactions 99 (2000) 110–116.
[9] D.R. Lide, CRC Handbook of Chemistry and Physics, 72nd ed., CRC Press, Boston, 1992.
[10] A. Capoglu, P.F. Messer, Design and development of a chamotte for use in a low-clay translucent whiteware, Journal of The European Ceramic Society 24 (2004) 2067–2072.
[11] A. Capoglu, A novel approach to high-strength, translucent whitewares using prefired materials, Key Engineering Materials 264–268 (2004) 1585–1588.
[12] A. Capoglu, M.U. Taskiran, Fabrication of low-clay containing translucent whiteware using prefired materials by slips casting, Key Engineering Materials 264–268 (2004) 1621–1624.
[13] M.U. Taskiran, N. Demirkol, A. Capoglu, A new porcelainised stoneware material based on anorthite, Journal of the European Ceramic Society 25 (2005) 293–300.
[14] A. Capoglu, M.U. Taskiran, Processing of ultra white porcelain stoneware based on anorthite, Key Engineering Materials 264–268 (2004) 1495–1498.
[15] C.B. Carter, M.G. Norton, Interacting with and generating light, Ceramics Materials Science and Engineering—Part VII (2007) 575–597.
[16] M.R. Meng, Q. Dou, Effect of pimelic acid on the crystallization, morphology and mechanical properties of polypropylene/wollastonite composites, Materials Science and Engineering: A 492 (2008) 177–184.
[17] A. Escardino, J.G. Ten, C. Feliu, A. Moreno, Calcium carbonate thermal decomposition in white-body wall tile during firing, Journal of the European Ceramic Society 30 (2010) 1989–2001.
[18] G. Sedmale, I. Sperberga, U. Sedmalis, Z. Valancius, Formation of high-temperature crystalline phases in ceramic from illite clay and dolomite, Journal of The European Ceramic Society 26 (2006) 3351–3355.
[19] P.T. Weon, K. Kimura, K. Jinnal, Fabrication of new porcelain body using nonplastic raw materials by slip casting, Journal of Materials Science 37 (2002) 1273–1279.
[20] K. Sedat, Y. Emre, A. Sedat, Effects of boron addition and intensive grinding on synthesis of anorthite ceramics, Ceramics International 34 (2008) 1629–1635.
[21] S. Kurama, E. Ozel, The influence of different CaO source in the production of anorthite ceramics, Ceramics International 35 (2009) 827–830.
[22] X.S. Cheng, S.J. Ke, Q.H. Wang, H. Wang, A.Z. Shui, P.A. Liu, Fabrication and characterization of anorthite-based ceramic using mineral raw materials, Ceramics International 38 (2012) 3227–3235.
[23] Annual Book of ASTM Standards, 2000, C-20, Standard Test Methods for Apparent Porosity, Water Absorption, Apparent Specific Gravity and Bulk Density of Burned Refractory Brick Shapes by Boiling Water.
[24] J.M.G. Ventura, D.U. Tulyaganov, S. Agathopoulos, J.M.F. Ferreira, Sintering and crystallization of akermanite-based glass–ceramics, Materials Letters 60 (2006) 1488–1491.
[25] F. Bouzerara, A. Harabi, S. Achour, A. Larbot, Porous ceramic supports for membranes prepared from kaolin and doloma mixtures, Journal of the European Ceramic Society 26 (2006) 1663–1671.
[26] Y. Chen, M. Wang, M. Hon, Phase transformation and growth of mullite in kaolin ceramics, Journal of African Earth Sciences 46 (2006) 245–252.
[27] S. Lagzdina, L. Bidermanis, J. Liepins, U. Sedmalis, Low temperature dolomitic ceramics, Journal of the European Ceramic Society 18 (1998) 1717–1720.
[28] S. Maity, B.K. Sarka, Development of high-strength whiteware bodies, Journal of the European Ceramic Society 16 (1996) 1083–1088.
[29] A. Doldstein, A. Gldenberg, M. Hefetz, Transparent polycrystallite $MgAl_2O_4$ spinel with submicron grains by low temperature sintering, Journal of the Ceramic Society of Japan 117 (2009) 1281–1283.
[30] V.M.F. Marques, D.U. Tulyaganov, S. Agathopoulos, V.Kh. Gataullin, G.P. Kothiyal, J.M.F. Ferreira, Low temperature synthesis of anorthite based glass-ceramics via sintering and crystallization of glass-powder compacts, Journal of the European Ceramic Society 26 (2006) 2503–2510.
[31] P. Rado, Bone China Ceramic Monographs, Handbook of Ceramics, Verlag Schmid GmbH, Freiburg i. Brg., 1981.
[32] R.K. Wood, Ceramic Whiteware, Ceramics and Glasses, Engineered Materials Handbook, ASM International, 1991.
[33] S.A.F. Batista, P.F. Messer, R.J. Hand, Fracture toughness of bone china and hard porcelain, British Ceramic Transactions 10 (2001) 256–259.
[34] H.L. Tang, J. Xua, H.J. Lia, Y.J. Dong, F. Wu, M.Q. Chen, Structure, thermal expansion and optical property of alumina-rich spinel substrate, Journal of Alloys and Compounds 479 (2009) 26–29.
[35] K. Yuichi, Y. Mitsunori, N. Mikio, O. Osamu, I. Hirofumi, Strength and thermal shock resistance of alumina-strengthened porcelain containing cristobalite, Journal of the Ceramic Society of Japan 111 (2003) 872–877.
[36] ICDD card of akermanite-synthetic 01-087-0052.
[37] D. Mousumi, P.S. Shiv, P. Karan, J. Suchika, K. Basudeb, Influence of combined Al_2O_3–SiO_2 filler on thermal and dielectric properties of barium zinc borate glass micro composites for barrier ribs of plasma display panels, Indian Journal of Engineering and Materials Sciences 17 (2010) 199–207.
[38] K.D. Swapan, D. Kausik, Differences in densification behavior of K- and Na- feldspar-containing porcelain bodies, Thermochimica Acta 406 (2003) 199–206.
[39] S.A. Berger, Practical Color Measurement: A Primer for the Beginner, a Reminder for the Expert, John Wiley, New York, 1994.
[40] A. Kara, R. Stevens, Characterisation of biscuit fired bone china body microstructure. Part I: XRD and SEM of crystalline phases, Journal of the American Ceramic Society 22 (2002) 731–736.
[41] C.B. Carter, M.G. Norton, Interacting with and generating light, Ceramics Materials Science and Engineering Part VII (2007) 575–597.
[42] N.B. Church, W.M. Johnson, Calculation of the refractive index of silicate glasses from chemical composition, Geological Society of America bulletin 91 (1980) 619–625.